PAPER

Nonthermal plasma synthesized silicon-silicon nitride core–shell nanocrystals with enhanced photoluminescence

To cite this article: Katharine I Hunter et al 2021 J. Phys. D: Appl. Phys. 54 504005

View the article online for updates and enhancements.

You may also like

- Gold nanorod/molybdenum sulfide core-shell nanostructures synthesized by a photo-induced reduction process Tien D Tran, Ly T Le, Dong H Nguyen et al
- Preparation of Hollow Titanium Dioxide Shell Thin Films by Electrophoresis and Electrolysis for Dye-Sensitized Solar Cells Masaya Chigane, Mitsuru Watanabe, Masanobu Izaki et al.
- Room-temperature ferromagnetic Crdoped Ge/GeO, core-shell nanowires Amar S Katkar, Shobhnath P Gupta, Md Motin Seikh et al.



J. Phys. D: Appl. Phys. 54 (2021) 504005 (8pp)

https://doi.org/10.1088/1361-6463/ac2695

Nonthermal plasma synthesized silicon-silicon nitride core-shell nanocrystals with enhanced photoluminescence

Katharine I Hunter, Himashi P Andaraarachchi and Uwe R Kortshagen*

Department of Mechanical Engineering, University of Minnesota, Minneapolis, MN 55455, United States of America

E-mail: kortshagen@umn.edu

Received 29 July 2021, revised 7 September 2021 Accepted for publication 14 September 2021 Published 28 September 2021



Abstract

Enhanced optical properties of silicon quantum dots (ODs) are pertinent for light-emitting applications including luminescent solar cell concentrators. Surface passivation plays a crucial role in improving photoluminescent quantum yield and effective carrier lifetimes of silicon nanocrystals and is often achieved by surface grafting of organic ligands. However, organically passivated silicon QDs often suffer from a deterioration of the optical properties when exposed to the environment. In this work, we explore the effect of an inorganic amorphous silicon nitride (SiN_x) shell on silicon QDs and their optical properties. Utilizing a dual plasma approach with dual injection ports, we synthesized Si/SiN_x core-shell nanoparticles using SiH₄, NH₃, H₂, and Ar. The core-shell nanocrystals were characterized using optical and structural methods, which revealed that higher nitridation plasma powers could lead to Si precipitation altering the composition of SiN_x shell. While as-synthesized Si/SiN_x core–shell nanocrystals did not exhibit photoluminescence, oxidized Si/SiN_x core–shell nanocrystals show significantly higher quantum yield (35%) and longer carrier lifetime compared to their bare oxidized Si analogues even after an environmental exposure of six months.

Supplementary material for this article is available online

Keywords: silicon, silicon nitride, core-shell nanocrystals, nonthermal plasma

(Some figures may appear in colour only in the online journal)

1. Introduction

Luminescent silicon quantum dots (QDs) are considered promising candidates for various light-emitting applications including luminescent solar concentrators [1-3]. Silicon is nontoxic and abundant and Si QDs have tunable optical properties ranging from visible to near-infrared (NIR) spectral region along with negligible overlap between the absorption and emission profiles, which enables high solar harvesting performance for luminescent solar concentrators [4, 5]. However, Si QDs are not as efficient emitters as traditional II-VI QDs, due to silicon's indirect bandgap, which requires phononassisted recombination [5]. Experimental efforts have shown that Si QDs emit light in the visible and NIR portion of the electromagnetic spectrum when their diameter is less than approximately 5 nm. Additionally, photoluminescence (PL) has been observed from films of Si QDs embedded in dielectric matrices, including silicon nitride (SiN_x) [6–9], silicon oxide (SiO_x) [10], and silicon oxynitride (SiO_xN_y) [10, 11],

Author to whom any correspondence should be addressed.

and have been intensely investigated for their use in optoelectronic applications.

The actual mechanisms involved in certain luminescence phenomena of Si QDs are still controversially discussed in the literature [12]. Silicon nanocrystals processed from high purity precursors in gas-phase processes, such as nonthermal plasmas, exhibit quantum confinement of carriers in the core of the nanocrystal, leading to size-dependent emission [13]. The wavelength of the emission shifts to higher energies with decreasing core dimensions. For light-emitting applications, the photoluminescence quantum yield (PLQY) should be maximized; thus, radiative recombination processes must be favored and non-radiative recombination processes minimized.

Experimental and theoretical evidence point to carrier recombination at defect sites on the nanoparticle surface as the most significant non-radiative process in intrinsic Si QDs [14, 15]. At the scale of quantum-confinement, upwards of 20% of atoms in the nanocrystal can be found within one unit cell of the nanoparticle surface. For this reason, surface passivation of light-emitting Si QDs is crucial for the fabrication of effective luminescent solar cell concentrators.

Popularly, surface passivation is achieved through organic termination of the silicon surface utilizing carboxylic acids [16], long chain hydrocarbons with terminal alkenes [17–19], aliphatic and aromatic amines [20], and bifunctional hydrocarbon chains [21]. However, in applications such as luminescent solar concentrators, where the long-term PLQY stability is important, it is generally found that the PLQY of organically passivated Si QDs decays upon exposure to the environment [3]. Inorganic surface passivation is inherently more stable. For bulk silicon devices, inorganic surface passivation has been intensely pursued, where this crucial process reduces surface recombination velocity and improves minority carrier lifetime in silicon solar cells for decades of exposure to the environment. A SiO_x passivating layer is traditionally used; however, recent PV devices have employed amorphous SiN_x as a passivating layer to optimize carrier transport [22–24].

In this work, we have adapted this concept and explored the use of an inorganic amorphous SiN_x , denoted a- SiN_x , as a passivant on Si QDs. The literature presents a complex picture of a- SiN_x . Often, films of a- SiN_x are described based upon their deposition conditions, for which the reported compositions and properties are poorly characterized or defined [25].

A key advance in colloidal QD engineering has been the development of methods for epitaxial shell growth in solution, notably successive ionic layer adsorption reaction [26] and colloidal atomic layer deposition [27], which allows for monolayer control over shell growth. However, these colloidal techniques have proven challenging to apply to group IV materials [28]

Nonthermal plasma reactors have emerged as a competitive synthesis technique to grow a library of nanomaterials including group IV nanocrystals [29, 30]. These plasma grown nanomaterials often offer improved morphology and uniformity due to high synthesis temperatures, enhanced purity due to lack of solvents, limited post-synthetic purification due to lack

of ligands, and elevated doping efficiencies due to kinetically driven growth.

Recent works have shown successful synthesis of several group IV core—shell nanostructures including Si/Ge [31] and Si/SiN_x core—shell nanocrystals [32, 33]. However, previous reports of plasma synthesized Si/SiN_x nanocrystals were produced using molecular nitrogen as a precursor. Both previous efforts reached similar conclusions that the SiN_x shell itself does not serve as an effective passivant nor does it prevent oxidation of silicon nanocrystals.

Herein, we explore the synthesis of quantum-confined Si QDs coated with an amorphous SiN_x shell utilizing SiH_4 , NH_3 , H_2 and Ar gases in a flow-through capacitively coupled non-thermal plasma reactor to investigate the impact of nitride coating on the QDs' optical performance. We employed a dual plasma approach with dual injection zones, which enables the tailoring of surface properties of Si QDs, including shell growth, before they have a chance to agglomerate [19, 32].

2. Methodology

2.1. Nanoparticle synthesis

Si QDs coated in an a-SiN_x shell were produced in a twostage, low-pressure nonthermal plasma. Silicon QD cores were grown in an upstream plasma analogous to the approach by [29] and then entered into a downstream Ar–NH₃ plasma for nitridation. Figure 1 shows the dual-plasma system used to synthesize Si QD with an a-SiN_x.

The primary gas feed, a mixture of argon (Ar), silane (SiH₄), and hydrogen (H₂), entered through the top of the 3/8"OD-1/4"ID borosilicate glass reactor tube. The plasma was generated in the reactor tube by the application of 10 W radiofrequency (RF) power at 13.56 MHz through a pair of copper ring electrodes, coupled through an impedence matching network. The distance separating the powered electrode from the grounded vacuum fitting below was 5 cm. The argon, silane, and hydrogen flow rates in the primary gas feed were fixed throughout this study at 31.4 sccm, 0.6 sccm, and 5 sccm, respectively, while the pressure was held at 2 Torr.

Downstream of the Si core growth region, the reactor expands to 1"OD-7/8"ID and an additional precursor was added through a second inlet to initiate shell growth. This secondary gas feed was composed of NH3 and Ar at fixed flowrates of 5 sccm each. This secondary gas feed was injected into the reaction chamber through a stainless steel vacuum fitting with 16 individual 1 mm diameter holes spaced evenly around the circumference of the reactor. The vacuum fitting itself was grounded and served as a counter electrode. Downstream of the secondary gas inlet, a second plasma was generated by the application of RF power at 13.56 MHz from a second power supply through a pair of copper ring electrodes, coupled through a second impedance matching network. The distance separating the powered electrode from the grounded vacuum fitting above was 4 cm. Within the second plasma, an a-SiN_x shell was grown through a nitridation process in which some fraction of the Si core was consumed and converted into

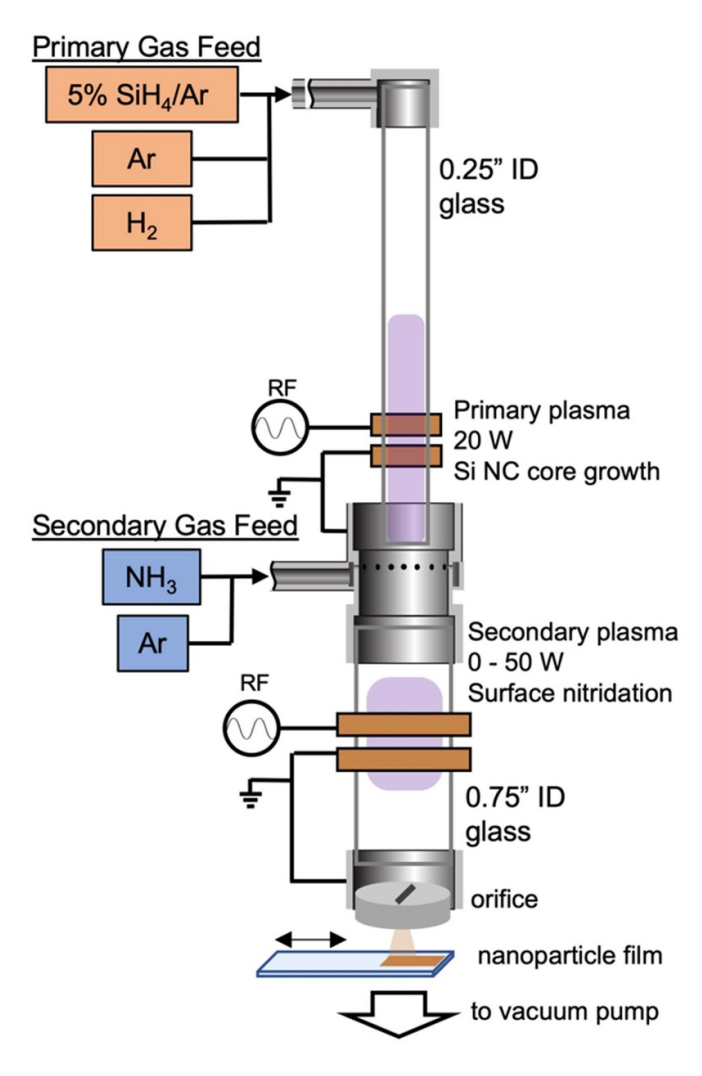


Figure 1. Schematic of reactor used for the synthesis of core/shell Si/a- SiN_x QDs.

the a-SiN_x shell. The residence time to grow these particles was estimated from the gas volumetric flow rate, the reactor diameter, and the length of the plasma region to be \sim 4 ms. Witness substrates were mounted to the chamber walls at various locations in the primary plasma and monitored for SiN_x film deposition to assess ammonia back diffusion. No SiN_x film deposition was observed upstream of the ammonia injection. We hypothesized that the back diffusion is substantially suppressed by the addition of an expansion region below the primary plasma.

2.2. Structural characterization

A combination of material characterization methods were required to infer dimensions and composition of the QD cores and shells. The structural analysis of these Si/a- SiN_x core/shell QDs is complicated by several factors including: the presence of silicon in both core and shell, minimal Z-contrast between core and shell, and sub 4 nm diameter, which makes imaging difficult. Therefore, a suite of material information

was collected including crystallite size from x-ray diffraction (XRD), optical bandgap estimates from UV–Vis absorption derived Tauc plots, surface species from Fourier transform infrared spectroscopy (FTIR), surface composition from x-ray photon spectroscopy (XPS), and optical properties from PL and time-resolved photoluminescence (TRPL) measurements. The combined information gleaned from these sources reveals the effects of applied power in the nitridation plasma on QD properties.

XRD was used to probe the dimensions of the crystalline silicon core as a means to estimate nitridation depth. Diffraction patterns were collected on a Bruker D8 Discover diffractometer with a beryllium 2D area detector using a Co–K α source (1.79 Å) and were mathematically converted to Cu–K α patterns (1.54 Å) for data analysis. Data analysis was performed using the Material Data Incorporated Jade 8.0 software package. Typical collection times were 10 min per frame. Samples were prepared directly from plasma synthesis by impaction from the gas phase onto glass microscope slides forming a nanoparticle film.

Absorption spectra were collected on a Cary 5000 spectrometer from QD films deposited on glass substrates at 0–50 W power in the nitridation plasma. The Tauc equation was used for the band gap estimation: $(\alpha h \nu)^{1/n} = \beta (h \nu - E_{\rm g})$, where α is the absorption coefficient of a material at a particular energy, $h\nu$, n=2 for an indirect-band gap semiconductor, and β is a proportionality constant. The indirect bandgaps, $E_{\rm g}$, were estimated by plotting $(\alpha h \nu)^{1/n}$ vs. $h \nu$ and extrapolating the first major absorption onset of the experimental data to the intersection with the baseline. The core sizes were derived from the Brus equation: $\Delta E(r) = E_{\rm g} + h^2/8r^2 (1/m_{\rm e}^* + 1/m_{\rm h}^*)$, where $E_{\rm g}$ is the band gap estimated from Tauc plots, h= Plank constant, r= radius of the QD, and $m_{\rm e}^*$ and $m_{\rm h}^*$ are effective masses of the excited electron and excited hole, respectively [34].

Mid-infrared absorption spectra were collected under inert conditions in a N₂-purged glovebox using a Nicolet spectrometer operated in diffuse-reflectance mode. Samples were prepared directly from plasma synthesis by impaction from the gas phase onto aluminum-coated Si wafers. Samples were not exposed to air prior to measurements.

XPS spectra were collected on a PHI VersaProbe III with a monochromatic Al $K\alpha$ anode x-ray source (photon energy = 1486.6 eV) and a hemispherical analyzer. All spectra were recorded using the PHI software package SmartSoftXPS v2.0 and processed using PHI MultiPack v9.0. Samples were deposited as nanoparticle films directly from plasma synthesis by impaction from the gas phase onto glass microscope slides. During analysis, sample neutralization was enabled.

Ideally, transmission electron microscopy (TEM) would be used to image the core—shell structures of the Si/a-SiN $_x$ QDs. This was attempted using an aberration-corrected scanning TEM (FEI Titan G2 60-300 at 200 keV). Unfortunately, due to the sub 4 nm size of the QDs considered here and due to the minimal Z-contrast between core and shell, this was inclusive. However, TEM studies of larger Si/a-SiN $_x$ nanocrystals produced in the same reactor, but under different

conditions, clearly confirmed the formation of a core–shell structure (figure S1 available online at stacks.iop.org/JPD/54/504005/mmedia).

The PLQY of a-SiN_x coated Si QD ensembles was characterized using the absolute measurement method where absorption and emission are recorded and integrated. Emission from photoluminescent Si QDs was measured using an Ocean Optics USB2000 spectrometer and integrating sphere. The absolute spectral response of the integrating sphere was calibrated using an Ocean Optics LS-1-CAL tungsten halogen light source. Rhodamine 101 dispersed in ethanol was used as a fluorescent standard to validate calibration. The excitation source was a 405 nm light-emitting diode. Samples were prepared as nanoparticle films directly from plasma synthesis by impaction from the gas phase onto glass microscope slides. The error associated with this absolute quantum yield measurement method is on the order of 5.5%. TRPL measurements were executed on a custom Horiba DeltaFlex system in rightangle alignment operated in multi-channel scaling mode, using a Horiba 405 nm pulsed laser diode operated at 2.0 mW, 50 ps, and 0.67 kHz repetition rate as the excitation source and a Horiba PPD-900 photon counting detector. Samples were prepared as nanoparticle films a few hundred nanometers in thickness directly from plasma synthesis by impaction from the gas phase onto glass microscope slides. Timeresolved spectral data were collected by taking decay curves at emission wavelengths from 550 to 900 nm in increments of 10 nm.

3. Results and discussion

Figure 2 exhibits the powder XRD patterns of Si/a-SiN_x particles and the crystallite sizes estimated by the Scherrer equation. The (111) peak at 28° was used to estimate the crystallite sizes. XRD patterns revealed crystalline Si cores (PDF 00-027-1402) for all applied powers in the second (nitridation) plasma. Specifically, we observe that the size of Si crystallite decreases with increasing power in the nitridation plasma, as illustrated in figure 2(c). This observation confirms that there is a monotonically increasing degree of consumption of the core Si QDs to form an amorphous SiN_x shell with increasing power in nitridation plasma. The lack of evidence for ammonia back diffusion in this system implies increased nitridation with increasing power in the nitridation plasma. Thus, we can conclude that the SiN_x shell thickness might increase with increasing power in nitridation plasma.

Interestingly, however, the absorption data display a different trend. Absorption spectra collected with varied power in the nitridation plasma were transformed to Tauc-plots and associated bandgap energies were estimated (figure S2 and table 1). From the Tauc plot derived Si core estimates, there is a drop in Si core size from 0 W (no nitridation) to 10 W. Nevertheless, at powers at 20 W and above, there is an apparent increase in the size of the Si core. It should be noted that while the Tauc-plot method to extract the optical bandgap of bulk materials is well-established [35], the literature shows questionable applicability to Si QD materials [36–38]. Therefore,

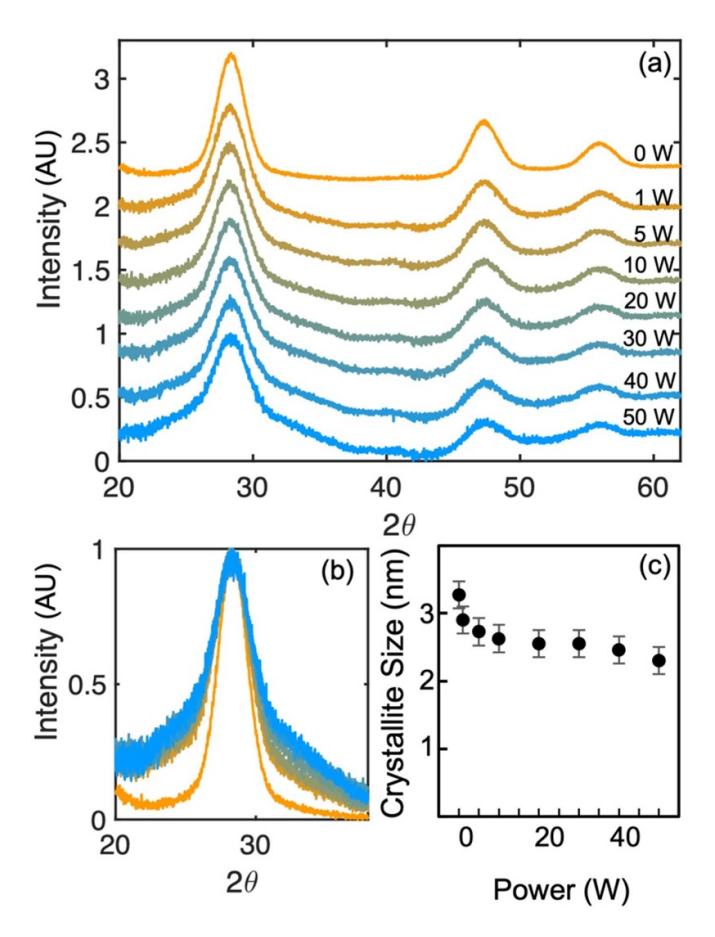


Figure 2. (a) Diffraction patterns for Si/a-SiN $_x$ core/shell QD synthesized under varying power in the nitridation plasma (0, 1, 5, 10, 20, 30, 40, 50 W). Spectra are offset for clarity. (b) The (111) diffraction peak of silicon overlaid for all samples for ease of comparison. (c) Crystallite sizes estimated from Scherrer broadening analysis are indicated for various powers in the nitridation plasma.

Table 1. Estimated band gaps and particle sizes of Si/a- SiN_x core–shell QDs synthesized under varied nitridation plasma power (0–50 W).

Power (2nd plasma)	Eg Tauc (eV)	Si core size (nm)
0 W	1.89	2.54
1 W	2.12	2.18
5 W	2.15	2.14
10 W	2.14	2.15
20 W	2.10	2.21
30 W	2.07	2.25
40 W	2.00	2.35
50 W	1.95	2.43

we used Tauc-plot derived bandgaps and particle sizes (table 1) to deduce trends rather than to conclusively determine Si QD core size.

We hypothesize that the apparent increase in Si core size above 20 W originates from precipitation of Si from the a-SiN_x coating due to increased nanoparticle heating by energetic surface reactions within the plasma at higher powers

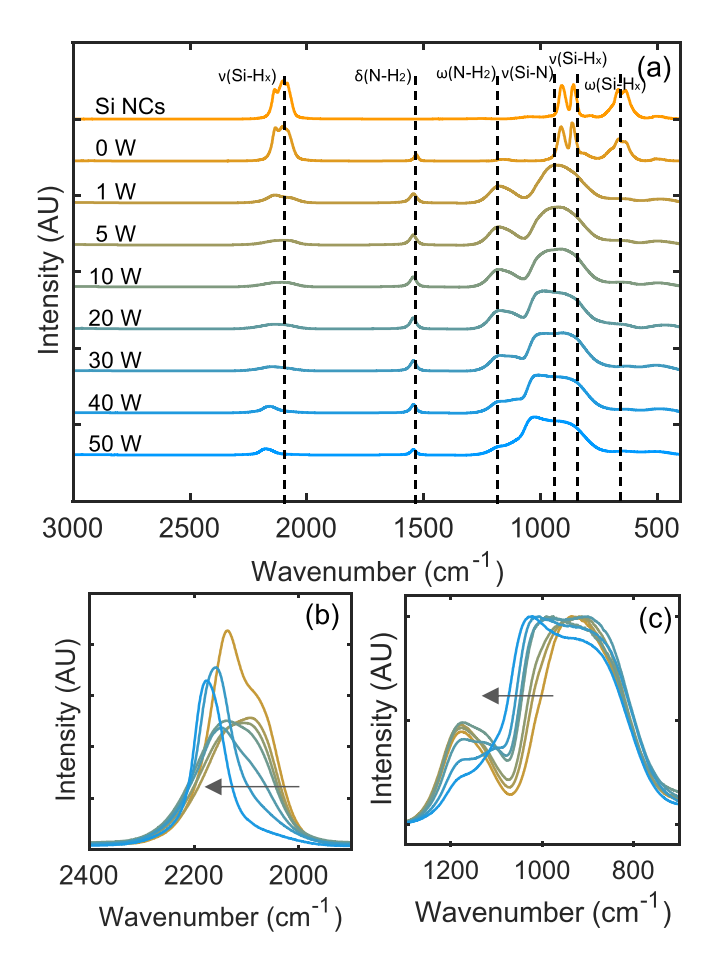


Figure 3. (a) FTIR spectra for Si/a-SiN_x core/shell QD synthesized for varying powers of nitridation plasma showing Si–H_x stretching modes at \sim 2050–2200 cm⁻¹, N–H₂ scissoring modes at \sim 1620 cm⁻¹, N–H₂ wagging modes at \sim 1200 cm⁻¹, Si–N asymmetric stretching modes at \sim 750–1000 cm⁻¹, Si–H_x deformation modes at \sim 800–1000 cm⁻¹, and Si–H₂ wagging modes at \sim 650 cm⁻¹. (b) Shift of Si–H_x vibration peaks to higher wavenumbers with increasing power of nitridation plasma. (c) Emergence of a shoulder around 1100 cm⁻¹ that indicates a reordering of SiN_x shell material during Si precipitation and increased SiN₄ bonding.

[39, 40]. The precipitation of Si in the form of nanoparticles from a-SiN_x films is a well-documented phenomenon, which can be induced under appropriate treatment processes [6–8]. Ultimately, this precipitation could lead to a nitrogen-rich SiN_x coating and an amorphous silicon interlayer deposited on the crystalline silicon core.

We performed FTIR measurements to investigate the surface composition of $Si/a-SiN_x$ core–shell particles and to test the above hypothesis of amorphous Si precipitation. Figure 3(a) shows the FTIR spectra for $Si/a-SiN_x$ core/shell nanoparticles synthesized under varying power in the second plasma. The broad peak around 750–1100 cm⁻¹ corresponds to the Si-N asymmetric stretching vibrations, which confirms SiN_x on the nanocrystal surface. Two peaks around ~ 1200 cm⁻¹ and ~ 1600 cm⁻¹ correlate to the N-H vibration modes. Above 10 W power in the nitridation plasma, a shoulder peak emerged between the 1000 and 1100 cm⁻¹

region associated with N_3 –(Si–N)–Si₂ configuration and silicon precipitation, which is consistent with prior literature [41, 42]. This provides evidence for the reordering of the SiN_x matrix that results during Si precipitation towards increased SiN₄ bonding and an increased ratio of N:Si in the shell (figure 3(c)). Thus, FTIR confirms that the apparent increase of Si core size determined by UV–Vis absorption is indicative of Si precipitation. Since no increase in core crystallite size is seen by XRD for powers above 10 W, the precipitate is amorphous.

The FTIR spectra also revealed a marked change in spectral features associated with hydrogen. As shown in figure 3(b), with increased power in nitridation plasma, peaks associated with $Si-H_x$ stretching modes that are located near 2100 cm⁻¹ were shifted to higher wavenumbers indicating increased N back-bonding forming *N–Si– H_x bonds [43]. This shift is consistent with increasing nitrogen content in shells produced at higher powers in the nitridation plasma [44].

The XPS spectra of the core/shell QDs exhibit peaks corresponding to N 1s and Si 2p features confirming the presence of nitrogen on the nanocrystal surface (figures S3 and S4). However, the N:Si ratio depends on the radius of the Si core and the thickness and composition of the SiN_x shell. Thus, we cannot use N:Si atomic ratio deduced by XPS to quantitatively determine shell composition or thickness.

Based on the above observations, we propose that two mechanisms to determine the nitridation of crystalline Si QDs under the studied conditions. The primary mechanism is that nitridation of Si QD surface in the second plasma reduces the core Si crystallite size. This is relevant at all powers in the secondary plasma. The secondary mechanism is that at higher nitridation powers, precipitation of an amorphous Si layer may lead to increased nitrogen concentration in the SiN_x shell. This pathway is more pronounced at nitridation plasma powers greater than 20 W.

The driving motivation behind this work is to explore the effect of an SiN_x shell on the optical properties of Si QDs. While PL from Si QDs is well documented, the photophysical processes that govern luminescence in Si QD ensembles are complicated. QD ensembles are polydisperse, radiative and non-radiative recombination rates are size-dependent, and inter-particle interactions, including exciton transport and processes, are complex and poorly understood in quantum-confined materials.

We performed PLQY measurements to characterize optical measurements. As-produced, there is no measurable PLQY for all samples synthesized at powers 0–50 W. However, upon exposure to atmosphere, the a-SiN_x shells began to oxidize and exhibit an appreciable PLQY. Over time, the PLQY increased until the shells reach a terminal oxide content and thickness. Samples were oxidized under ambient atmospheric conditions for six months and PLQY was periodically measured. Figure S5 shows the progression of PLQY for samples produced at selected powers (0, 1, 20, and 50 W). Hydrogen-terminated Si QDs, produced at 0 W in the nitridation plasma, exhibit a slow onset to PLQY and reach a maximum quantum yield of around 15%. In contrast, the Si/a-SiN_x core/shell QDs produced at 1 W in the nitridation plasma rapidly exhibit moderate

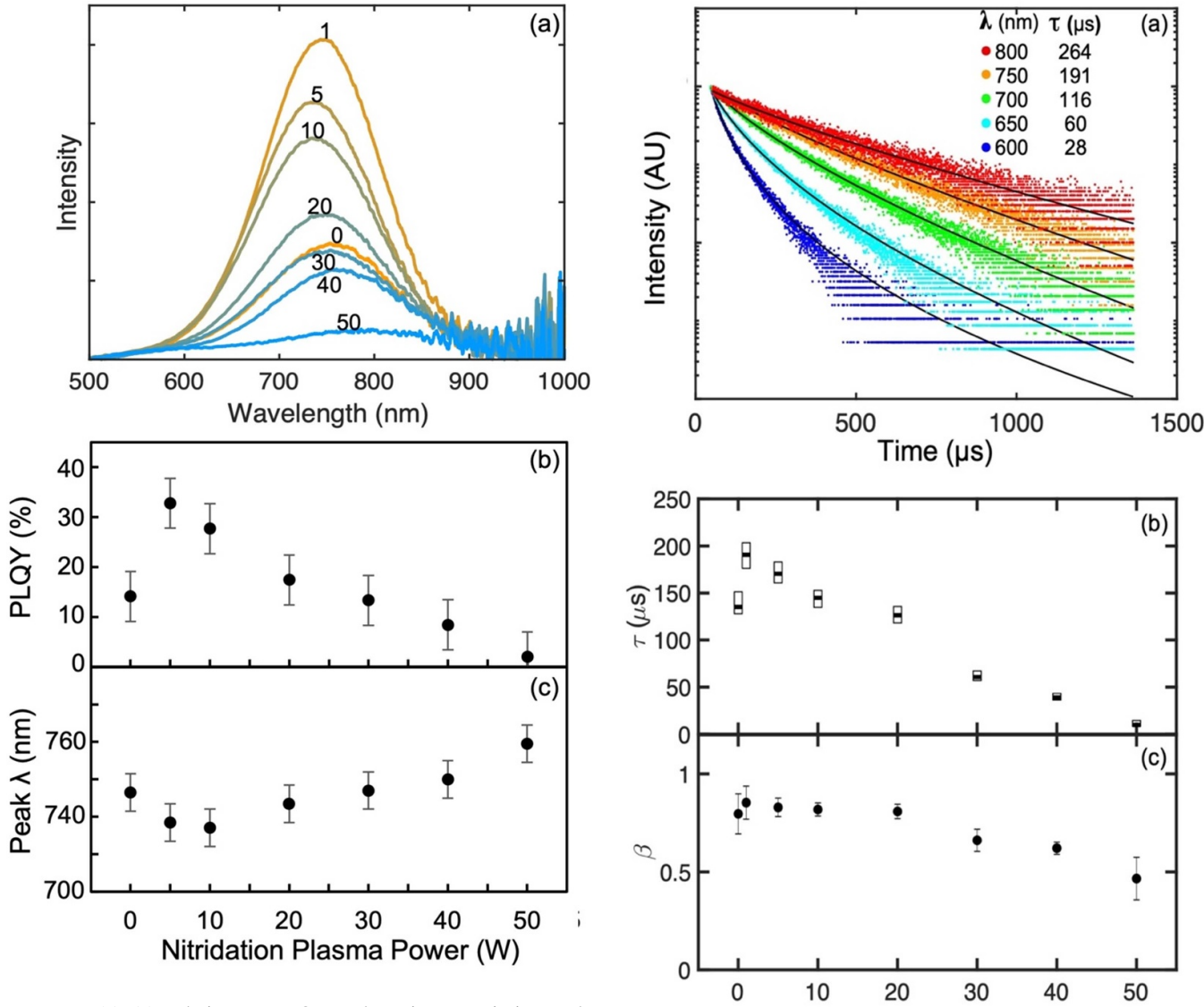


Figure 4. (a)–(c) Relative PL, PLQY, and maximum emission peak wavelength for all samples produced at varied nitridation plasma powers (0, 1, 5, 10, 20, 30, 40, 50 W) after six months of oxidation.

quantum yields within the span of a few days and reaches a maximum quantum yield of more than 30%. As power in the nitridation plasma was increased, the rate of increase in PLQY and maximum quantum yield after six months were both reduced.

Figures 4(a) and (b) present the relative PL spectra and PLQY of samples produced at varied nitridation plasma powers (0, 1, 5, 10, 20, 30, 40, 50 W) after six months of oxidation. Si/a-SiN_x core/shell QDs produced at 1 W nitridation plasma exhibited the highest relative PL and PLQY after six months. At nitridation plasma powers of 20 W and higher, both the relative PL and the PLQY were decreased indicating an increase in defect concentration within the Si QD ensemble. We suggest that at these powers, the formation of an amorphous Si interlayer on the crystalline Si core resulting from Si precipitation could contribute to increasing defect density.

Figure 4(c) demonstrates the maximum peak emission wavelengths after six months oxidation for samples under

Figure 5. (a) Decay curves from a Si/a-SiN_x core/shell ensemble produced at 1 W power in the nitridation plasma with emission wavelength range of 600–800 nm. (b) and (c) the effective life times (τ) and stretching exponents (β) of core/shell samples produced at varied nitridation plasma powers at 750 nm emission wavelength.

Nitridation Plasma Power (W)

varying power in the second plasma (0, 1, 5, 10, 20, 30, 40, 50 W). For quantum confined Si QDs, the peak emission wavelength is directly related to the size of the QD. The trend in peak emission wavelength, which blueshifts from 0 to 10 W and then redshifts at higher powers, is consistent with the trend seen in optical absorption spectra (figure S2). These results also confirmed the proposed amorphous Si precipitation, which creates an a-Si interlayer at powers of 20 W and greater, increasing the effective core Si size. Precipitation of amorphous Si at higher powers was feasible due to the increased nanoparticle heating by energetic surface reactions within the plasma.

Time-resolved spectral data were collected by taking decay curves at emission wavelengths from 600 to 800 nm in

increments of 50 nm. Figure 5(a) shows a decay curve from a Si/a-SiN_x core/shell ensemble produced at 1 W power in the nitridation plasma with emission wavelength range of 600–800 nm. After nearly six months of oxidation, these core/shell QDs showed the longest effective carrier lifetime τ of 264 μ s and the highest stretching exponent value $\beta \sim 0.85$. Figures 5(b) and (c) presented the effective life times and stretching exponents of core/shell samples produced at varied nitridation plasma powers at 750 nm emission wavelength. Consistent with PLQY measurements, there is a relative degradation in optical properties for Si/a-SiN_x QDs produced at increasing nitridation plasma powers. Specifically, with increased power in the nitridation plasma, the QD ensembles exhibited shorter effective carrier lifetimes and lower β values.

The rapid process of oxidation for $Si/a-SiN_x$ QDs is similar to the oxidation of $a-SiN_x$ prepared by plasma enhanced vapor deposition (PECVD) [45, 46]. In the PECVD process, films prepared at low-temperature result in a low-density, porous, 'fractal-like network' which permits air and moisture to percolate, resulting in a much shorter timescale for the full conversion of $a-SiN_x$ films to $a-SiO_xN_y$ than for films produced at higher temperatures which are composed of higher density $a-SiN_x$. For $Si/a-SiN_x$ QDs produced at 1 W power, we hypothesize that a low-density, porous $a-SiN_x$ shell provides a means for rapid vacancy oxidation to an $a-SiO_xN_y$ shell that is thicker than found from the oxidation of H-terminated Si QD under ambient conditions.

Thus, post-oxidation, the a-SiO $_x$ N $_y$ for samples produced below 20 W power in the nitridation plasma provides improved surface passivation for Si QDs relative to passivation by native oxide. Further work will be conducted to for process optimization to evaluate the effectiveness of a-SiO $_x$ N $_y$ coating across a range of Si QD sizes and emission energies.

4. Conclusions

Si QDs coated with an amorphous SiN_x shell were formed in a two-stage, capacitively coupled plasma reactor utilizing SiH₄, NH₃, H₂, and Ar. As the nitridation plasma power increased, it was found that crystallite Si core sizes were decreased indicating consumption of the crystalline Si core forming an amorphous SiN_x shell. However, Tauc-plots derived from UV-Vis absorption spectra exhibited an increase in Si core size above 10 W of nitridation plasma power. We hypothesized that silicon precipitation can occur from a-SiN_x shell forming an amorphous Si interlayer with N-rich SiN_x shell contributing to the larger Si core sizes, which was reported in the prior literature. This was confirmed by the emergence of a shoulder peak at 1100 cm⁻¹ in FTIR spectra, which is attributed to the reordering of the SiN_x matrix forming N₃-(Si-N)-Si₂ bonding during Si precipitation. XPS spectra revealed peaks corresponding to Si 2p and N 1s confirming the presence of Si and N in the shell material.

While as produced Si/a- SiN_x core/shell ensemble did not exhibit PL right after synthesis, oxidized particles showed appreciable PL with PLQY as high as 35% even after six months of exposure to the environment. Upon oxidation,

Si/a-SiN_x core—shell QDs produced at 1 W nitridation plasma power showed the highest PLQY, the longest carrier life time with the largest exponential stretch exponents of 0.85. Corroborating the above observations, optical properties of these QD ensembles including relative PL, PLQY, effective carrier life time, and stretching exponent values decreased with the increasing plasma nitridation power. This is consistent with the Si precipitation forming an amorphous Si interlayer at higher nitridation plasma powers, which would lead to the increased surface defect density and degradation of optical properties. Furthermore, we conclude that post oxidation of low-density porous a-SiN_x shells, produced below 20 W of nitridation plasma power, permits rapid oxidation to form a-SiO_xN_y shells, which serve as a stable passivant improving the optical properties.

Data availability statement

The data that support the findings of this study are available upon reasonable request from the authors.

Acknowledgments

K Hunter acknowledges support by the National Science Foundation Graduate Research Fellowship Program under Grant No. 00039202. H Andaraarachchi and U Kortshagen acknowledge support by the U.S. Army Research Office under MURI Grant W911NF-18-1-0240. This work was supported by the U.S. National Science Foundation through the University of Minnesota MRSEC under Award Number DMR-1420013. Parts of this work were carried out in the Characterization Facility, University of Minnesota, which receives partial support from NSF through the MRSEC program.

Conflict of interest

The authors declare no conflicts of interest.

ORCID iD

Uwe R Kortshagen https://orcid.org/0000-0001-5944-3656

References

- [1] Cheng K-Y, Anthony R, Kortshagen U R and Holmes R J 2011 Nano Lett. 11 1952–6
- [2] Ng W L, Lourenco M A, Gwilliam R M, Ledain S, Shao G and Homewood K P 2001 Nature 410 192–4
- [3] Meinardi F, Ehrenberg S, Dhamo L, Carulli F, Mauri M, Bruni F, Simonutti R, Kortshagen U and Brovelli S 2017 Nat. Photon. 11 177–85
- [4] Meier C, Gondorf A, Lüttjohann S, Lorke A and Wiggers H 2007 J. Appl. Phys. 101 103112
- [5] Delerue C, Allan G and Lannoo M 2001 Phys. Rev. B 64 193402
- [6] Dal Negro L, Yi J H, Kimerling L C, Hamel S, Williamson A and Galli G 2006 Appl. Phys. Lett. 88 183103

- [7] Ma K, Feng J Y and Zhang Z J 2006 Nanotechnology 17 4650–3
- [8] Scardera G, Puzzer T, Perez-Wurfl I and Conibeer G 2008 J. Cryst. Growth 310 3680–4
- [9] Wang M, Li D, Yuan Z, Yang D and Que D 2007 Appl. Phys. Lett. 90 131903
- [10] Yang M-S, Cho K-S, Jhe J-H, Seo S-Y, Shin J H, Kim K J and Moon D W 2004 Appl. Phys. Lett. 85 3408–10
- [11] Molinari M, Rinnert H and Vergnat M 2000 Appl. Phys. Lett. 77 3499–501
- [12] Sinelnikov R, Dasog M, Beamish J, Meldrum A and Veinot J G C 2017 ACS Photonics 4 1920–9
- [13] Sykora M, Mangolini L, Schaller R D, Kortshagen U, Jurbegs D and Klimov V I 2008 *Phys. Rev. Lett.* **100** 067401
- [14] Wu J J and Kortshagen U R 2015 RSC Adv. 5 103822-8
- [15] Brawand N P, Voros M and Galli G 2015 Nanoscale 7 3737–44
- [16] Hua F, Swihart M T and Ruckenstein E 2005 *Langmuir* 21 6054–62
- [17] Buriak J M 2002 Chem. Rev. 102 1271–308
- [18] Jurbergs D, Rogojina E, Mangolini L and Kortshagen U 2006 Appl. Phys. Lett. 88 233116
- [19] Mangolini L and Kortshagen U 2007 Adv. Mater. 19 2513–9
- [20] Dasog M, De Los Reyes G B, Titova L V, Hegmann F A and Veinot J G 2014 ACS Nano 8 9636–48
- [21] Yu Y, Hessel C M, Bogart T D, Panthani M G, Rasch M R and Korgel B A 2013 Langmuir 29 1533–40
- [22] Chowdhury Z R, Cho K and Kherani N P 2012 Appl. Phys. Lett. 101 021601
- [23] Kim J W and Yeom H W 2003 Phys. Rev. B 67 035304
- [24] Shi X, Shriver M, Zhang Z, Higman T and Campbell S J 2004 Vac. Sci. Technol. A 22 1146–51
- [25] Kaloyeros A E, Jov'e F A, Goff J and Arkles B 2017 ECS J. Solid State Sci. Technol. 6 P691–714
- [26] Dabbousi B O, Rodriguez J, Mikulec F V, Heine J R, Mattousi H, Ober R, Jensen K F and Bawendi M G 1997 J. Phys. Chem. B 107 9463–75

- [27] Ithurria S and Talapin D V 2012 J. Am. Chem. Soc. 134 18585–90
- [28] Guo Y, Rowland C E, Schaller R and Vela J 2014 *ACS Nano* **2014** 8334–43
- [29] Mangolini L, Thimsen E and Kortshagen U 2005 Nano Lett. 5 655–9
- [30] Kortshagen U R, Sankaran R M, Pereira R N, Girshick S L, Wu J J and Aydil E S 2016 Chem. Rev. 116 11061–127
- [31] Hunter K I, Held J T, Mkhoyan K A and Kortshagen U R 2017 ACS Appl. Mater. Interfaces 9 8263–70
- [32] Weeks S L, Leick N and Agarwal S 2015 Plasma Process. Polym. 13 116–23
- [33] Mandal R, OShea K and Anthony R 2018 J. Vac. Sci. Technol. A 36 051303
- [34] Brus L E 1984 J. Chem. Phys. 44 4403-9
- [35] Tauc J 1968 Mat. Res. Bull. 3 37-46
- [36] Hao X J, Cho E-C, Flynn C, Shen Y S, Conibeer G and Green M A 2008 *Nanotechnology* **19** 424019
- [37] Dung M X, Tung D D, Jeong S and Jeong H-D 2013 Chem. Asian J. 8 653–64
- [38] Huang C-H, Wang X-Y, Igarashi M, Murayama A, Okada Y, Yamashita I and Samukawa S 2011 Nanotechnology 22 105301
- [39] Mangolini L and Kortshagen U 2009 Phys. Rev. E 79 026405
- [40] Kramer N J, Anthony R J, Mamunuru M, Aydil E S and Kortshagen U R 2014 J. Phys. D: Appl. Phys. 47 075202
- [41] Scardera G, Puzzer T, Conibeer G and Green M A 2008 *J. Appl. Phys.* **104** 104310
- [42] Debieu O, Nalini R P, Cardin J, Portier X, Perrière J and Gourbilleau F 2013 *Nanoscale Res. Lett.* **8** 1–13
- [43] Lucovsky G, Yang J S, Chao J T and Czubatyj W 1983 Phys. Rev. B 28 3234–40
- [44] Parsons G N and Lucovsky G 1990 Phys. Rev. B 41 1664-7
- [45] Kaloyeros A E, Pan Y, Goff J and Arkles B 2020 ECS J. Solid State Sci. Technol. 9 063006
- [46] Takeyama M B, Sato M, Nakata Y, Kobayashi Y, Nakamura T and Noya A 2014 Japan. J. Appl. Phys. 53 05GE01